Influences of biomass burning during the Transport and Chemical Evolution Over the Pacific (TRACE-P) experiment identified by the regional chemical transport model

Youhua Tang,[1] Gregory R. Carmichael,[1] Jung-Hun Woo,[1] Narisara Thongboonchoo,[1] Gakuji Kurata,[2] Itsushi Uno,[3] David G. Streets,[4] Donald R. Blake,[5] Rodney J. Weber,[6] Robert W. Talbot,[7] Yutaka Kondo,[8] Hanwant B. Singh,[9] and Tao Wang[10]

Received 31 October 2002; revised 18 April 2003; accepted 25 April 2003; published 4 November 2003.

[1] Using a regional chemical transport model, STEM 2K1, and the emission inventory for the Transport and Chemical Evolution Over the Pacific (TRACE-P) period [*Woo et al.*, 2003 *Streets et al.*, 2003], we successfully simulated important features of the biomass burning (BB) CO outflow. Simulated results agree well with the TRACE-P aircraft measurements and Thailand surface observations. On the basis of sensitivity studies with and without biomass emissions, we identified nine flight segments that are affected by biomass plumes during the TRACE-P period and compared the characteristics of the BB air masses with the other air masses. The BB air masses emitted from Southeast Asia contain relatively high HCN ($\Delta HCN/\Delta CO \sim 0.0015$) and potassium ($\Delta K^+/\Delta CO \sim 0.0038$) but very low NO_y ($\Delta NO_y/\Delta CO \sim 0.005$) mixing ratios, which may be associated with the special burning condition in this region. The biomass burning air masses have high ozone production efficiency. The observed $\Delta O_3/\Delta NO_z$ values were ~17 in biomass events and 1.7 in other events. The BB influence on the trace gas distributions can be divided into two categories: the influence through direct reactions and the influence caused by BB aerosols changing *J* values. These two influences are discussed for the BB-affected TRACE-P flights and for east Asia. The BB influences on chemical species are not only determined by the BB plume intensity but also by the ambient environment caused by other emissions. In Southeast Asia, where the biogenic emissions are very strong, the OH background concentration is low, and the BB gas-phase compounds mainly contribute to OH production. Arranged in the sensitivity to the *J* value change caused by BB aerosols, we have $OH > HO_2 > HCHO > O_3$ when evaluated on a regional average. Averaged over March, the biomass burning net influence is as high as 50% for OH, 40% for HO_2, 60% for HCHO, and 10 ppbv for O_3 for the layers below 1 km. *INDEX TERMS:* 0305 Atmospheric Composition and Structure: Aerosols and particles (0345, 4801); 0322 Atmospheric Composition and Structure: Constituent sources and sinks; 0345 Atmospheric Composition and Structure: Pollution—urban and regional (0305); 3337 Meteorology and Atmospheric Dynamics: Numerical modeling and data assimilation; 3359 Meteorology and Atmospheric Dynamics: Radiative processes; *KEYWORDS:* biomass burning, chemical transport model, TRACE-P, photochemical process, aerosols, radiative influence

Citation: Tang, Y., et al., Influences of biomass burning during the Transport and Chemical Evolution Over the Pacific (TRACE-P) experiment identified by the regional chemical transport model, *J. Geophys. Res.*, *108*(D21), 8824, doi:10.1029/2002JD003110, 2003.

1. Introduction

[2] It is widely recognized that biomass burning (BB) emissions are a major source of tropospheric gas and aerosol pollutants. *Galanter et al.* [2000] estimated that biomass burning emissions account for 15–30% of the entire tropospheric CO background. BB emitted CO is about twice that from fossil fuel combustion on the global scale [*Holloway et al.*, 2000]. Biomass burning is also an important source of aerosols.

[1]Center for Global and Regional Environmental Research, University of Iowa, Iowa City, Iowa, USA.
[2]Department of Ecological Engineering, Toyohashi University of Technology, Toyohashi, Japan.
[3]Research Institute for Applied Mechanics, Kyushu University, Fukuoka, Japan.
[4]Argonne National Laboratory, Argonne, Illinois, USA.
[5]Department of Chemistry, University of California at Irvine, Irvine, California, USA.
[6]School of Earth and Atmospheric Sciences, Georgia Institute of Technology, Atlanta, Georgia, USA.
[7]Institute for the Study of Earth, Oceans, and Space, University of New Hampshire, Durham, New Hampshire, USA.
[8]Research Center for Advanced Science and Technology, University of Tokyo, Tokyo, Japan.
[9]NASA Ames Research Center, Moffett Field, California, USA.
[10]Department of Civil and Structural Engineering, Hong Kong Polytechnic University, Hong Kong, China.

0148-0227/03/2002JD003110$09.00

[3] The Transport and Chemical Evolution Over the Pacific (TRACE-P) field experiment was performed with two aircrafts (NASA DC8 and P3B) from early March to early April of 2001, a traditional season of biomass burning in Southeast Asia. During the TRACE-P period, aircraft measurements indicated that biomass burning emissions were a big contributor to CO, black carbon (BC), organic carbon (OC), and HCN in this region. Satellite images also showed that fires frequently appeared in Southeast Asia; and synoptic weather reports recorded frequent "haze" weather, a signal of biomass burning smog. The strong BB influence in this region is not only identified by TRACE-P experiment, but also by previous experiments [*Maloney et al.*, 2001].

[4] It is difficult to quantify the BB influences directly through measurements alone. East Asia is the most populous region in the world, and is also largely a main developing region. This region has very high anthropogenic emissions, in which biofuel emissions play a large role [*Woo et al.*, 2003]. Since the burning materials are similar, it is not easy to distinguish the biomass burning and biofuel pollutants just based on chemical analysis. In fact, it is also not easy to divide the contribution of biomass burning from fossil fuel burning, because most of the plumes observed by TRACE-P aircrafts contain mixtures of emission sources. Three-dimensional models can help evaluate the BB influences for this period.

[5] In this paper, we use a three-dimensional model to simulate the role of biomass burning, and compare to the TRACE-P measurements and some surface station data. On the basis of these simulations, we evaluate the direct and indirect influences of biomass burning on TRACE-P flights and on the region as a whole.

2. Methodology

[6] We employed the STEM 2K1 [*Tang et al.*, 2003] regional chemical transport model to make simulations for this period. The STEM model has a detailed chemical mechanism (SAPRC 99) and explicit photolysis solver (NCAR Tropospheric Ultraviolet-Visible radiation model). This model was successfully used for TRACE-P simulations and calculated values compared well with the observed data [*Carmichael et al.*, 2003; *Tang et al.*, 2003]. The biomass emissions used in this study are described by *Woo et al.* [2003]. *Streets et al.* [2003] describe our anthropogenic emissions in detail.

[7] For this study, we performed two simulations: one with and another without biomass burning emissions, named NORMAL, and NOBIOM, respectively. The NORMAL simulation is our baseline run, and considers all emissions, deposition, gas-phase chemistry, transport, diffusion, and aerosol influences on photolysis rates. This simulation is the same as the baseline simulation presented in *Tang et al.* [2003] and *Carmichael et al.* [2003]. In this study, we did not consider the role of heterogeneous reactions on aerosol surfaces. The NOBIOM simulation is the same, except the emissions from open burning sources were set to zero.

3. Biomass Burning CO Identified by Observations and Simulations

[8] CO is an important species to represent the evidence of biomass burning, since this species has a large BB emission source, and can be transported over long distances. Figure 1 shows the estimated total biomass burning CO emission rate [*Woo et al.*, this issue] of Southeast Asia, including Burma, Thailand, Vietnam, Laos and Cambodia, derived from fire count information. Biomass burning emissions are highly uncertain, and must be evaluated. Since the strongest impacts of biomass burning are in the source areas, we choose that area for the emissions evaluation. Figure 1 shows the comparisons of CO concentrations at four Thailand regional stations, located in the north of Thailand. The NORMAL simulation agrees well with the surface measurements, and successfully captured the BB CO peak on 8 March (the 67th Julian day). The differences between the NORMAL and NOBIOM simulations indicate that the contribution from BB CO is as high as 3 ppm. The BB CO emission in this region reached a maximum on 7 March. The CO concentration peaked one day later, as indicated by both the modeled and observed results. Figure 1 also shows the simulated CO concentrations and observed CO by *Wang et al.* [2003] in a Hong Kong suburban site. Hong Kong was not a biomass burning source area, but sometimes was strongly affected by biomass burnings. BB emissions contributed up to 300 ppb of CO to this site during TRACE-P period. The strongest BB plume emitted from Southeast Asia on 7 March arrived at Hong Kong and caused the CO peak concentration on 12 March (the 71st Julian day). Our later analysis will discuss the transport route of this plume and its influence on TRACE-P flights.

[9] The strong biomass burning emissions from Southeast Asia can have a large influence on the TRACE-P aircraft measurements. By comparing model results with the aircraft data, we identified nine flight periods where the BB signals were significant, as shown in Figure 2. Figure 2 indicates that the NORMAL simulation agrees well with the observed CO concentrations, and the NOBIOM results significantly underestimate CO concentrations for these nine flight segments. The corresponding BB CO horizontal distributions, wind fields, and flight paths are presented in Figure 3 at the major altitudes of these flights.

[10] Figure 3 shows most BB plumes initially headed northeast when they departed from the source areas of Southeast Asia, and were driven by the seasonal monsoon. From 7 to 10 March, a cold front was the main weather activity in this region. Five TRACE-P flights sampled the evolution of this front during this period. The frontal wind system transported the biomass burning and anthropogenic pollutants from west to east, and formed a clear band with a high concentration of pollutants. Most BB pollutants were exported to the west along the warm conveyor belt associated with this front. Behind this front, the high-pressure system brought clear air from high altitude to the lower layers, and generated a large CO gradient across the front. The five TRACE-P flights (P3 flight 9, 10, 11, and DC8 flight 7, 8) encountered the strongest BB CO plumes. As shown for P3 flight 9 (Figure 2), the BB CO contribution was up to 200 ppbv, which nearly doubled the background CO concentrations at some locations. This feature was also captured in a similar altitude range (from 2 to 6 km) by the DC8 flight 7. Our trajectory analysis points out that the high CO concentrations of both the P3 flight 9 and DC8 flight 7 came from Southeast Asia after traveling 2–3 days.

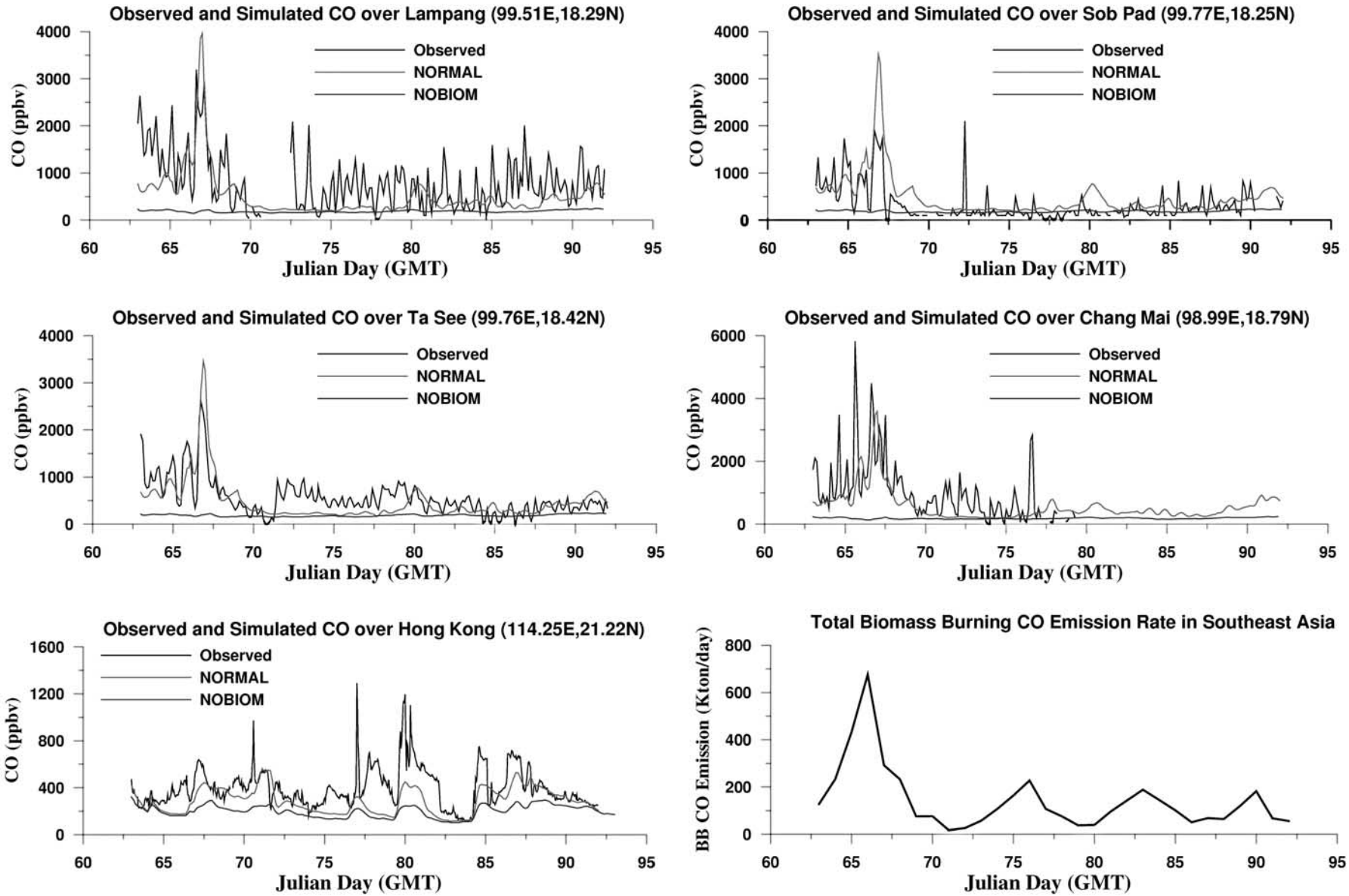

Figure 1. Observed and simulated CO concentrations over four Thailand surface stations and Hong Kong and estimated biomass CO emissions in Southeast Asia during the TRACE-P period. The Lampang, Sob Pad, and Ta See surface stations are located in rural sites, and the Chang Mai and Hong Kong stations are the suburban sites. See color version of this figure at back of this issue.

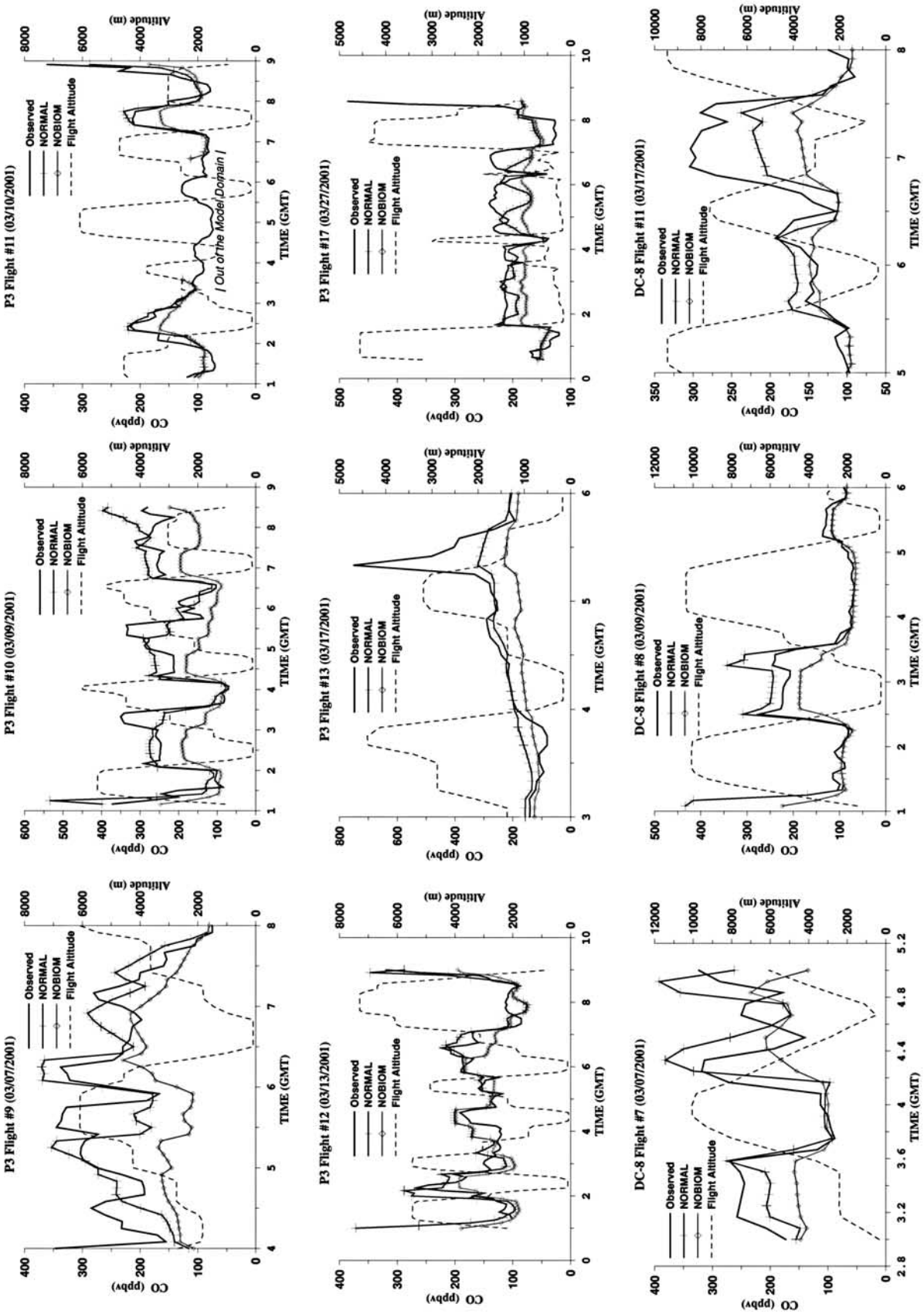

Figure 2. Observed CO compared to NORMAL and NOBIOM simulations for flight segments identified as high-biomass influences. See color version of this figure at back of this issue.

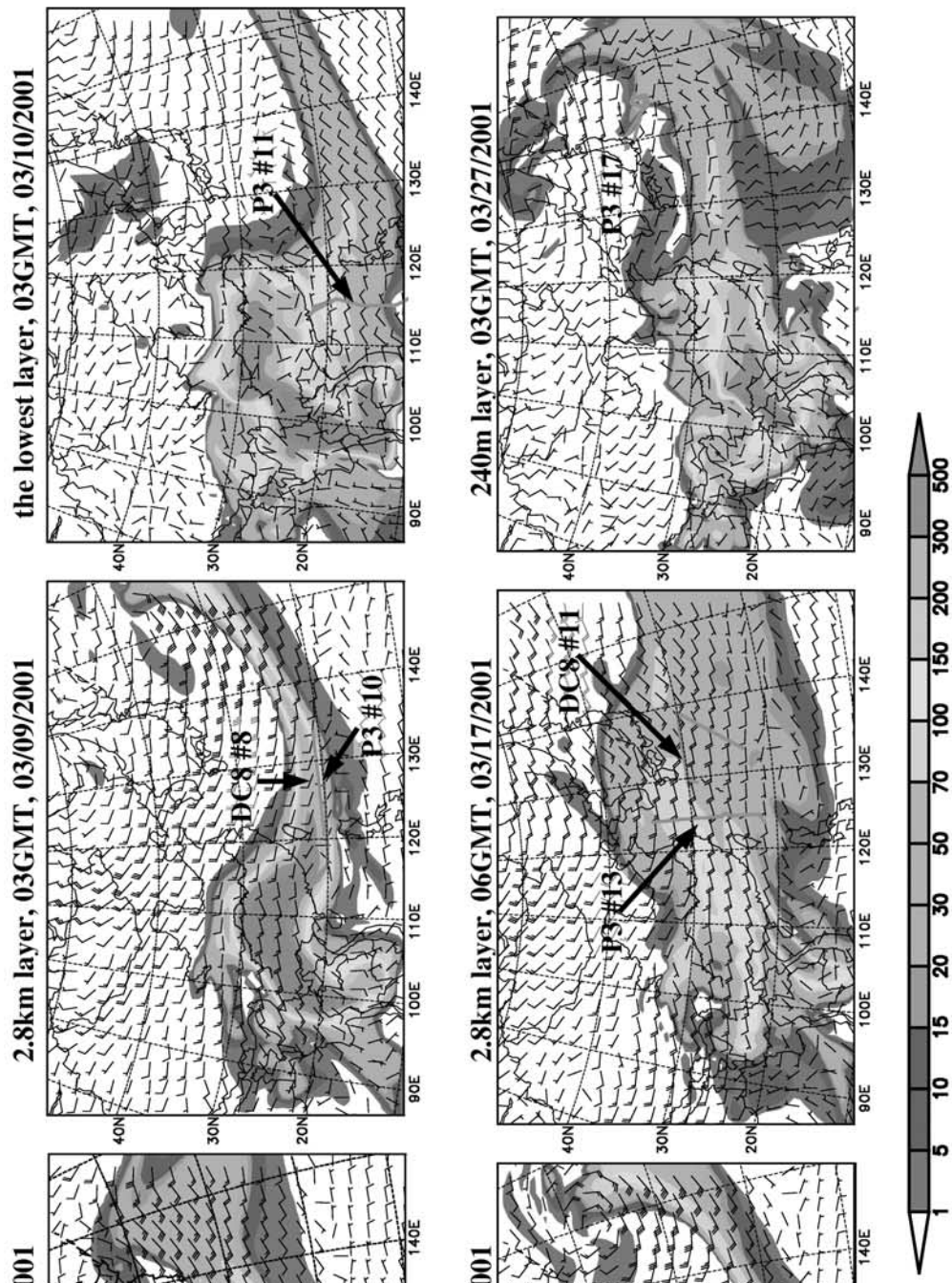

Figure 3. Simulated biomass burning CO concentrations at the major altitudes for the nine flights shown in Figure 2. The red lines refer to the flight paths mentioned in Figure 2. See color version of this figure at back of this issue.

[11] On 9 March, the cold front moved to 20°N. As shown in Figure 3, both the P3 flight 10 and the DC8 flight flew along the 20°N latitude line, with a purpose to observe the continental outflow brought by the front. Figure 2 shows that BB CO affected the trace gas distributions along the P3 and DC8 paths at these times. This BB influence was concentrated in the layers from 2 to 4 km. This situation implies that the air masses below and above 2 km may come from different sources. Our backward trajectory verifies this fact. Owing to the complex frontal structure and stratification, the air mass was clearly divided, with air masses arriving at 2–4 km coming from Southeast Asia, and the air masses below 2 km carrying pollutants emitted from northern China. The BB air mass from 2 to 4 km altitudes departed from northern Thailand on 7 March when the biomass burning emissions in Southeast Asia reached a maximum. The absolute CO concentration at that departing location was about 800 ppbv. Although this concentration is much lower than the peak concentration appearing in the same location one day later, as shown in Figure 1, it still contributed significant CO enhancements along the aircraft flight paths.

[12] On 10 March, the cold front nearly decayed. In the decaying region of the front, the high-pressure system transported aged BB air masses to the surface when it moved to the downwind areas, and was encountered by the P3 flight 11. The purpose of this flight was to measure the air mass of the marine boundary layer. This flight encountered aged BB air masses at low altitudes. Our analysis shows that that low-altitude biomass air mass did not come from Southeast Asia directly, but stayed over the East China Sea for more than 5 days. Although the BB air mass is very aged, its CO signal is still sufficiently strong to affect the CO concentrations. One day later (Julian day 71), this widespread BB recirculation air mass resulted a CO peak in Hong Kong (Figure 1).

[13] On 13 March, there was another cold front that passed along 20°N. The BB air mass encountered by the P3 flight 12 was also transported along the warm conveyor belt of the front. The transport situation is similar to that on 9 March, and the high BB CO also appeared at an altitude of ~3 km. However, the flight path was different. The flight path crossed over the front line, and entered the postfront high-pressure system. The biomass burning signals lasted only 1 hour, in the P3 back-and-forth flight path.

[14] Both P3 flight 13 and DC8 flight 11 encountered significant BB CO signals on 17 March over the East China Sea and the western Pacific Ocean. A weak cold front existed and extended from the northeast to Taiwan, but its influence on the flights was not strong. This situation was a typical monsoon-driven transport system. The prevailing southwest monsoon transported BB air mass in the northeast direction from the surface to about 4 km. Biomass burning affected nearly the entire P3 flight 13, and contributed a CO enhancement of about 50 ppbv. The BB-affected area was quite broad, and covered nearly the entire western Pacific from 15° to 40°N. Biomass burning provided an enhanced "background" of CO concentration to this region. This background overlapped with the Shanghai plume, as indicated by the P3 observation.

[15] The P3 flight 17 encountered a low-altitude aged BB air mass on 27 March. The original purpose of this flight was to measure the volcanic plume emitted from Mt. Miyakajima. So this flight kept a low altitude (mostly below 500 m). Although the NORMAL simulation underestimated the CO concentration at some locations, the widespread biomass burning influence contributed about 50 ppbv of CO to the background. At the same day (Julian day 87) in the south region (Figure 3), a BB plume from Southeast Asia caused a CO peak in Hong Kong (Figure 1).

4. Observed Biomass Burning Features

[16] The TRACE-P flight paths are far way from the biomass burning source region. Our trajectory analysis indicates that the BB air masses take at least two days to arrive at the aircraft locations during these scenarios. On its transport way, the biomass burning plume may also mix with other emissions, since other sources in the region are also strong. Even though the model and observations clearly identified the BB CO signatures in the flights mentioned above, the BB features sometimes are still not strong enough to be distinguished from background and other influences. Here we resample the nine flight periods with simulated BB CO. When the BB CO concentrations are higher than 60 ppbv, we define the scenarios as "biomass burning events", which includes about 140 data points in the 5 min merged data set. We define all TRACE-P scientific flight periods other than the nine BB-affected periods as "other events" for comparison purpose.

[17] Figure 4 shows the observed correlations of CO versus HCN (Hydrogen Cyanide), K^+ (potassium), NO_y and C_2H_2 (ethyne) during biomass burning and other events. The observed HCN is only available for DC-8 flights [*Singh et al.*, 2003], and the other species in Figure 4 were observed by both aircrafts. These species have relatively long lifetimes, so we can use this information to examine the original emission signals.

[18] The BB air masses tend to have higher $\Delta HCN/\Delta CO$ and $\Delta K^+/\Delta CO$ ratios, and lower $\Delta NO_y/\Delta CO$ and $\Delta C_2H_2/\Delta CO$ ratios than the air masses from other sources (mainly anthropogenic emissions). The slopes of HCN versus CO are 0.0015 for BB events and 0.0011 for other events. This BB slope is much higher than that measured in biomass burning plumes in Australian tropical savannas during the 1991 and 1992 dry seasons by *Hurst et al.* [1994], which was about 0.00028. Their air masses were sampled in the near-source area. This difference reflects regional differences in the biomass burning characteristics. The BB $\Delta K^+/\Delta CO$ slope (0.0038) is also higher than that measured over the Indian Ocean, 0.0029, by *Reiner et al.* [2001]. *Reiner et al.* [2001] mentioned that their samples might contain both biomass burning and biofuel signals. Since the BB events that we define here are the very strong scenarios of biomass burning, it is possible that the India and Southeast Asia have similar K^+/CO BB emission ratios. The biggest slope difference between biomass burning and other events are seen for the values of $\Delta NO_y/\Delta CO$, and the slope in the other events is about 3 times that in the BB events. *Hurst et al.* [1994] reported that the $\Delta NO_x/\Delta CO$ value in savannas biomass burning was about 0.023, which is even higher than the $\Delta NO_y/\Delta CO$ slope in the other events for the TRACE-P flights. Their observed $\Delta C_2H_2/\Delta CO$ ratio was about 0.00072, which is 50 times smaller than that in

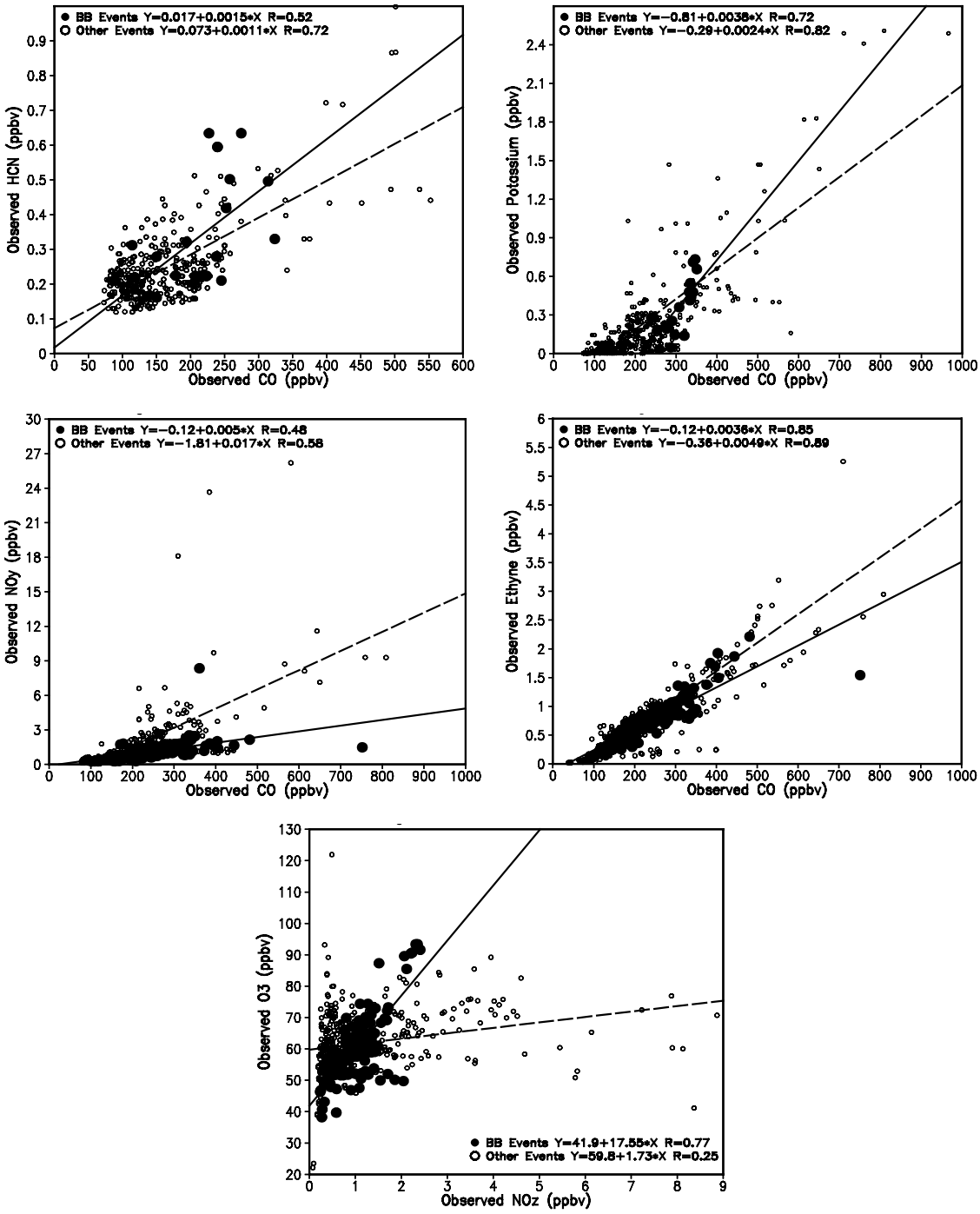

Figure 4. Observed correlations of CO versus HCN, potassium, NO_y, and ethyne and of O_3 versus NO_z in biomass burning and other events. The closed circles and solid fit lines refer to the BB events, and the small open circles and dashed fit lines represent the other events.

TRACE-P BB events (0.0038). The other events of TRACE-P flight have an even higher $\Delta C_2H_2/\Delta CO$ value (0.0049). The dynamic mixing along the transport path can affect the BB slopes sampled by the TRACE-P aircrafts, depending on the ambient concentrations. The air mass slopes reflect the mixing results of BB and anthropogenic air mass. However, the slope differences between BB and other events do suggest the tendency of the biomass burning emission ratios. It also shows that the BB air masses emitted from Southeast Asia have lower $\Delta NO_y/\Delta C_2H_2$ than that in the savannas BB plumes [*Hurst et al.*, 1994], which implies their difference on NO_x/VOC emission ratio.

[19] These results indicate that the biomass burning in Southeast Asia and Australian tropical savannas belong to different types. Australian tropical savannas are relatively dry, and have higher burning temperature, and the burning is relatively complete. These conditions benefit the production of nitrogen oxidants, but reduce the emission rates

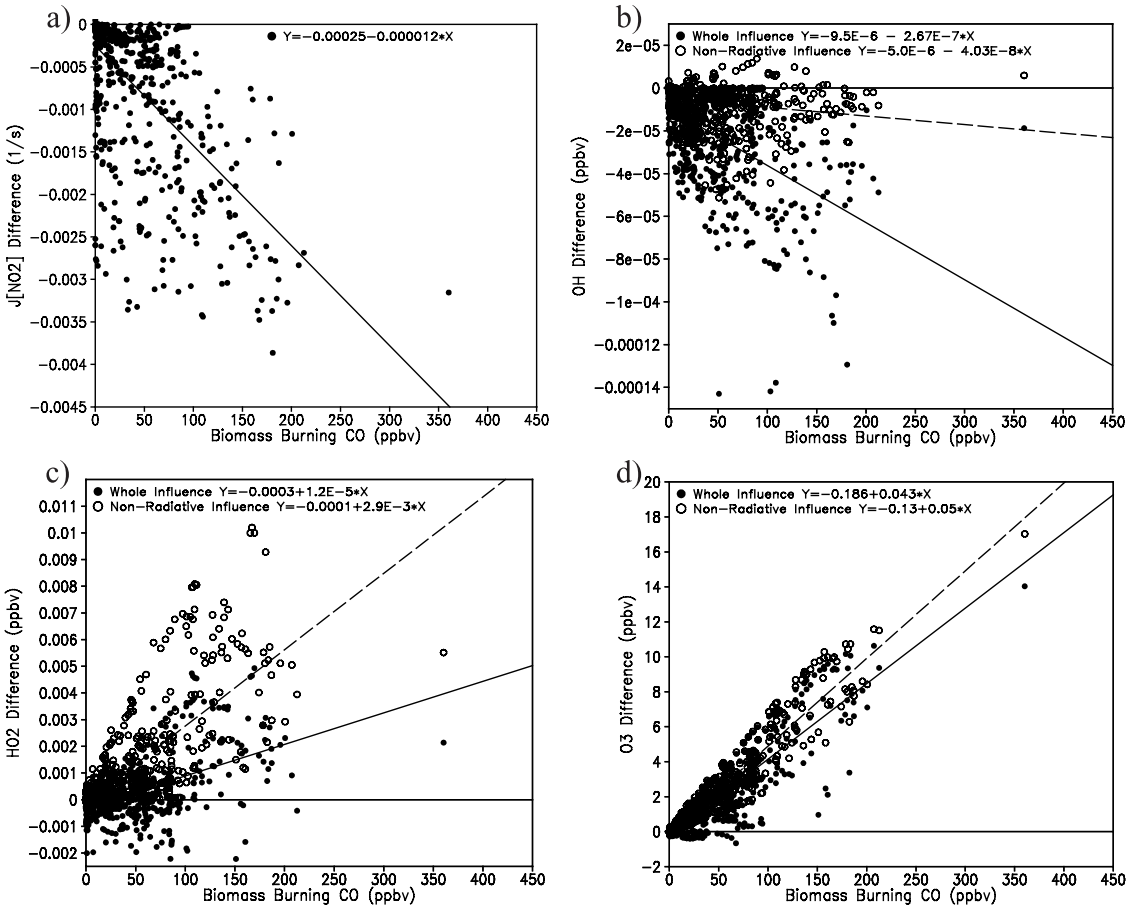

Figure 5. Simulated biomass burning net and nonradiative influences on (a) $J[NO_2]$, (b) OH, (c) HO_2, and (d) O_3 versus biomass CO during the nine biomass-affected periods of TRACE-P flights.

of VOC (volatile organic compound) and HCN. The biomass burning in Southeast Asia represents a contrary situation. This region in the monsoon season is very humid, and the combustion efficiency in tropical forests should be relatively incomplete. The TRACE-P observations show that these BB plumes contain very low nitrogen oxidants, but are rich in VOCs. The air mass characteristics bring a totally different regional O_3 producing scenario. NO_z ($NO_y - NO_x$) is the oxidized products of NO_x, including peroxyacetyl nitrate (PAN), HNO_3, HNO_2 et al. The ratio O_3/NO_z represents the upper limit of the ozone production efficiency (OPE) per unit NO_x [*Trainer et al.*, 1993]. Figure 4 shows that the $\Delta O_3/\Delta NO_z$ value (17.55) in the BB events is 10 times that (1.73) in other events. The biomass burning air masses emitted from Southeast Asia have very high OPE.

5. Other Biomass Burning Influences on TRACE-P Flights

[20] The influence of biomass burning emissions on gas-phase chemistry of this region can be divided into two parts: the influence via radiative forcing, and the nonradiative influence. *Tang et al.* [2003] found that BC and OC aerosols imposed a significant impact on regional radiation transfer, and reduced primary photolysis rates by up to 60% in low altitudes. This impact further affects regional photochemistry. The biomass burning are the main supplier of BC and OC south of 30°N in this region. To distinguish the biomass burning influences due to radiative effects, we ran another simulation that was the same as the NORMAL case, but without biomass burning aerosols (we call this the "NOBAOD"). The difference between NORMAL and NOBAOD represents the BB influence via photolysis processes, the difference between NOBAOD and NOBIOM represents the BB nonradiative influence, and the difference between NORMAL and NOBIOM shows the net biomass burning influence.

[21] Figure 5 shows the BB influences on $J[NO_2]$ (NO_2 photolysis rate), OH, HO_2, and O_3 plotted against the BB contribution to CO during the selected nine BB-affected periods. The $J[NO_2]$ reduction is not due to CO enhancement, but due to biomass burning aerosols in these BB-affected periods. BB aerosols contain black carbon (BC), organic carbon (OC) and potassium, and these particles are coemitted and transported with gaseous compounds. The concentrations of BB aerosol are usually proportional to BB CO, and emission factors for biomass burning are often referenced to CO. The existence of BB aerosols can affect the photolysis rates below and above them. Since the BB aerosol contains BC, it is strongly radiatively absorptive, and causes the J values to decrease [*Tang et al.*, 2003]. The observed data of aerosol single scattering albedo (SSA) show high variability. The average

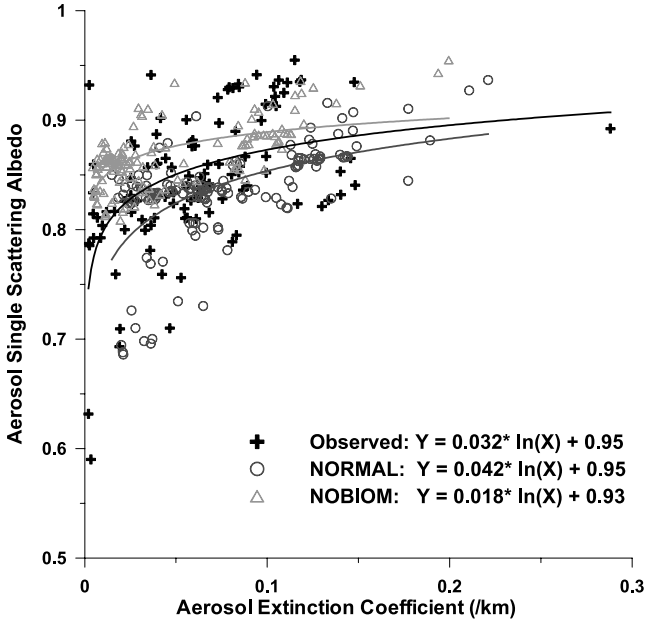

Figure 6. The observed and simulated correlations between aerosol single scattering albedo and extinction coefficient during the biomass burning events (BB CO > 60 ppbv). See color version of this figure at back of this issue.

value of observed SSA was 0.82 for the selected nine BB-affected periods, and the NORMAL simulation yielded a value of 0.83, and the NOBIOM simulation had a value of 0.84. In strong biomass burning events, the SSA change due to BB aerosol is higher. Figure 6 shows the correlations between SSA and aerosol optical extinction coefficient (AOE) during the biomass events, as defined in section 4. The NORMAL simulation slightly overestimated the aerosol absorption, and caused an underestimation of SSA. The simulation without biomass burning significantly overestimated SSA by missing some low SSA values.

[22] The effect on photolysis processes is not only caused by local aerosols, but also by the aerosol loadings below or above that arise from other sources. As a result, the $J[NO_2]$ reduction sometimes is not directly proportional to local BB aerosol loading. From Figure 5, we can see that the existence of BB aerosols generally causes $J[NO_2]$ to decrease. Other J values, e.g., $J[O_3 \rightarrow O_2 + O(^1D)]$, behave in a similar manner. Since OH is highly sensitive to $J[O_3 \rightarrow O_2 + O(^1D)]$, OH decreases due to BB aerosols. The CO and VOC enhancements due to biomass burning emissions can also cause an OH reduction through the reaction

$$\text{(R1)} \qquad CO(R \cdot H) + OH + O_2 \rightarrow HO_2(RO_2) + CO_2(H_2O).$$

Here we use $R \cdot H$ to represent the general form of VOC in photochemical reactions, and R represents alky radicals. The CO and VOC have a similar impact on OH reactions and photochemically production of O_3, though VOC reactions are more complex and need several steps to complete. When we exclude the radiative impact, reaction (1) becomes the main influence of BB air masses on OH, and contributes to OH reduction. Figure 5b shows that sometimes OH concentrations increase under the BB nonradiative influence. The reason is that BB CO and VOC increase O_3 levels in aged biomass burning air masses, and this O_3 contributes to the OH production via

$$\text{(R2)} \qquad HO_2(RO_2) + NO \rightarrow NO_2 + OH(RO);$$

$$\text{(R3)} \qquad NO_2 + h\nu \rightarrow NO + O^3P;$$

$$\text{(R4)} \qquad O^3P + O_2 \rightarrow O_3;$$

$$\text{(R5)} \qquad O_3 + h\nu \rightarrow O_2 + O(^1D);$$

$$\text{(R6)} \qquad O(^1D) + H_2O \rightarrow 2OH.$$

Reactions (1)–(6) should result in an increase of OH. However, these reactions are constrained by the NO_x availability and J values. After long distance transport, the BB air masses usually have low NO_x concentrations, and reaction (1) overwhelms the other reactions, causing OH to decrease in the aged BB plumes. Our analysis shows that most of the OH enhancements due to the nonradiative influence in Figure 5b occur at about 0600 GMT, when the O_3 production and J values reached their maximum values.

[23] Under the biomass burning nonradiative influence, HO_2 increased (Figure 5c) due to reaction (1). When adding the radiative influence, HO_2 sometimes decreased due to radiative-reduced OH. So the net biomass influence on HO_2 is determined by the BB CO concentration and J value changes due to BB aerosols. In most of the nine BB-affected flight segments, the former influence was stronger.

[24] Reactions (1)–(4) show how BB CO and VOC leads to increases in O_3. It should be noted that most O_3 enhancements in Figure 5d are not due solely to local O_3 production increases. These O_3 enhancements are accumulated along the transport journey of the biomass air masses, since O_3 is also a relatively long-lived species. Also because of the long lifetime, the O_3 enhancement remains in well-aged biomass burning air masses. As shown in Figure 3, biomass burning provides a wide range of CO enhancements in east Asia. These plumes have higher OPE and are NO_x limited. In Asia, BB plumes often pass over regions with significant NO_x emissions, and thus O_3 production can be sustained for long periods. The TRACE-P flights captured the signal of regional O_3 enhancement due to biomass burning. Figure 5d shows that the BB radiative influence restrains O_3 production, and sometimes turns the net BB influence on O_3 to negative. It also implies that reaction (3) is stronger than reaction (5) in the lower troposphere, since J value reduction mostly leads to O_3 reduction. Overall, the impact of BB aerosols on O_3 via affecting photolysis rates is much weaker than the biomass influence on O_3 due to direct reactions, as indicated by the small slope difference of Figure 5d.

6. Biomass Burning Regional Influences

[25] The discussions above focused on the influences of biomass burning on trace gases measured along the

TRACE-P flight paths. Figure 2 presented six scenarios of BB CO outflows during this period. *Tang et al.* [2003] show the aerosol influences on *J* values, OH, and O_3 in regional scale. In that paper, most aerosol influences south of 25°N are due to biomass burning. Our analysis shows that both radiative and nonradiative influences of biomass burning are concentrated in the layer below 4 km. Most biomass burning signals captured by TRACE-P flights also appeared in these layers.

[26] Figure 7 shows the simulated March-averaged net BB influences on daytime OH, HO_2 and HCHO below 1 km and from 1 to 3 km. On average, the OH decrease due to BB influence is as great as 40% below 1 km, and up to 35% from 1 to 3 km. The biggest OH decrease occurs not in the biomass burning areas, but in the downwind locations. The background OH in Southeast Asia is low because this region also has strong biogenic emissions. Under these conditions, reaction (1) becomes weak, and the BB nonradiative influence on OH becomes positive. In this region, the BB nonradiative influence can enhance OH concentrations by up to 90%. In the downwind regions, where the biogenic emissions are not so strong during this season, the BB nonradiative influence on OH turns to negative. The BB aerosol influence always leads to reduced photolysis rates and OH. This influence is mainly determined by the BB aerosol optical depth, and appears the strongest in the biomass burning areas. Our analysis indicates that in Southeast Asia, the nonradiative and radiative influences are of the same order of magnitude. Downwind, the radiative influence is usually much stronger than the nonradiative influence on OH, and both of them lead to decrease OH concentrations. On average, the radiative influence on OH is stronger than the nonradiative effects. The net biomass burning influence on OH, combined by both of these influences, mainly exists south of 35°N, and becomes weak with height (Figure 7).

[27] The BB influence on HO_2 has some features similar to OH. Our analysis shows that the BB nonradiative influence on HO_2 is positive. The radiative influence on daytime HO_2 is always negative, since the influence on OH is also negative. The net BB influence is determined by the strengths of these two components, and has a geographic distribution similar to that of OH. The net influence on HO_2 is positive in most biomass burning areas except in northern Thailand, and becomes negative in most downwind areas. In the horizontal direction, the biomass nonradiative influence on HO_2 decays faster than the radiative influence along the transport route. In the vertical direction below 3 km, the biomass nonradiative influence decays slower than the radiative influence along the vertical enhancement. The difference between these two influences reflects the following fact: the nonradiative influence is mainly determined by the local chemical compound's concentrations, and the radiative influence mostly depends on the aerosol optical thickness. The radiative influence is more sensitive to altitude change than the nonradiative influence since the BB plume can elevate up to the middle troposphere, and the latter is more sensitive to the dilution of BB compounds than the former. On the regional average, these two influences on HO_2 are of the same order of magnitude.

[28] Our sensitivity study shows that both nonradiative and radiative influences of biomass burning contribute to increasing formaldehyde (HCHO) concentrations. The reason that the nonradiative process increases formaldehyde is because biomass burning also emits significant amounts of VOCs, and HCHO is one of the main products of VOC oxidation. In biomass burning regions, the HCHO production is very high. It should be noted that the background HCHO in Southeast Asia is also high due to strong biogenic emissions, and this is identified by the GOME (Global Ozone Monitoring Experiment) satellite observation (see website: http://www-as.harvard.edu/chemistry/trop/tracep/hcho_tp.jpg). Under these conditions, the photolysis processes mainly lead to HCHO destruction. So reducing *J* values results in higher HCHO concentrations, and the BB radiative influence on HCHO appears positive. This radiative influence is usually weaker than the nonradiative influence. For example, in the altitude below 1 km, the nonradiative process can enhance HCHO up to 55%, and the radiative influence contributes to HCHO increase up to 20%.

[29] Reactions (3) and (4) are the main sources of photochemically generated ozone. So, reductions of *J* values lead to O_3 decreases. Figure 8 shows that biomass burning aerosols can reduce O_3 by up to 5 ppbv below 1 km, and 3 ppbv from 1 to 3 km by reducing *J* values. The BB nonradiative process can cause O_3 enhancements of more than 10 ppbv in the layers below 3 km. The biomass burning influences on low-layer O_3 also depend on the NO_x concentrations. In the strong BB plumes that mix with few other air masses, the NO_x/VOC and NO_x/CO ratios were very low, but the OPE is very high. The widespread BB plumes usually mix with some high-NO_x anthropogenic pollutants. So, in general, the O_3 production caused by biomass burning was not constrained by NO_x availability, and the BB nonradiative influence on O_3 keeps positive. Figure 8 shows that near source areas, the BB nonradiative influence below 1 km is stronger than that from 1 to 3 km, represented by that the former has a bigger area where this influence is higher than 10%. In our simulations, the biomass burning emission was treated as a elevated source, and its altitude variation below 3 km was relatively insignificant in our 80 km horizontal resolution. So the concentrations of BB CO etc had no strong altitude variation below 3 km. However, most high-NO_x anthropogenic emissions belong to surface sources, and were concentrated in the near-surface layer. The different nonradiative influences on O_3 between these two layers represent the altitude variation of high-NO_x anthropogenic pollutants in the BB source area. *Carmichael et al.* [2003] indicated that as a region with low NO_x/VOC ratio, Southeast Asia is more sensitive to NO_x increase than to VOC increase for O_3 enhancement. In most places, the BB net influence on O_3 is also positive. Only in the middle and lower reaches of the Yangtze River, including Shanghai, does the BB net influence turn to be slightly negative in the layer below 1 km. As a populous region, the Yangtze River surrounding areas have very high anthropogenic emissions. Compared to these strong local emissions, the BB CO and VOCs transported from Southeast Asia become insignificant, especially in Shanghai plume. Under that circumstance, the influence of BB aerosols on photochemical processes may be slightly higher than the BB nonradiative O_3 production. On a regional average, the BB nonradiative influence on O_3 is much higher than the radiative influence. For March, the biomass burning causes an O_3 enhancement band in south of 30°N,

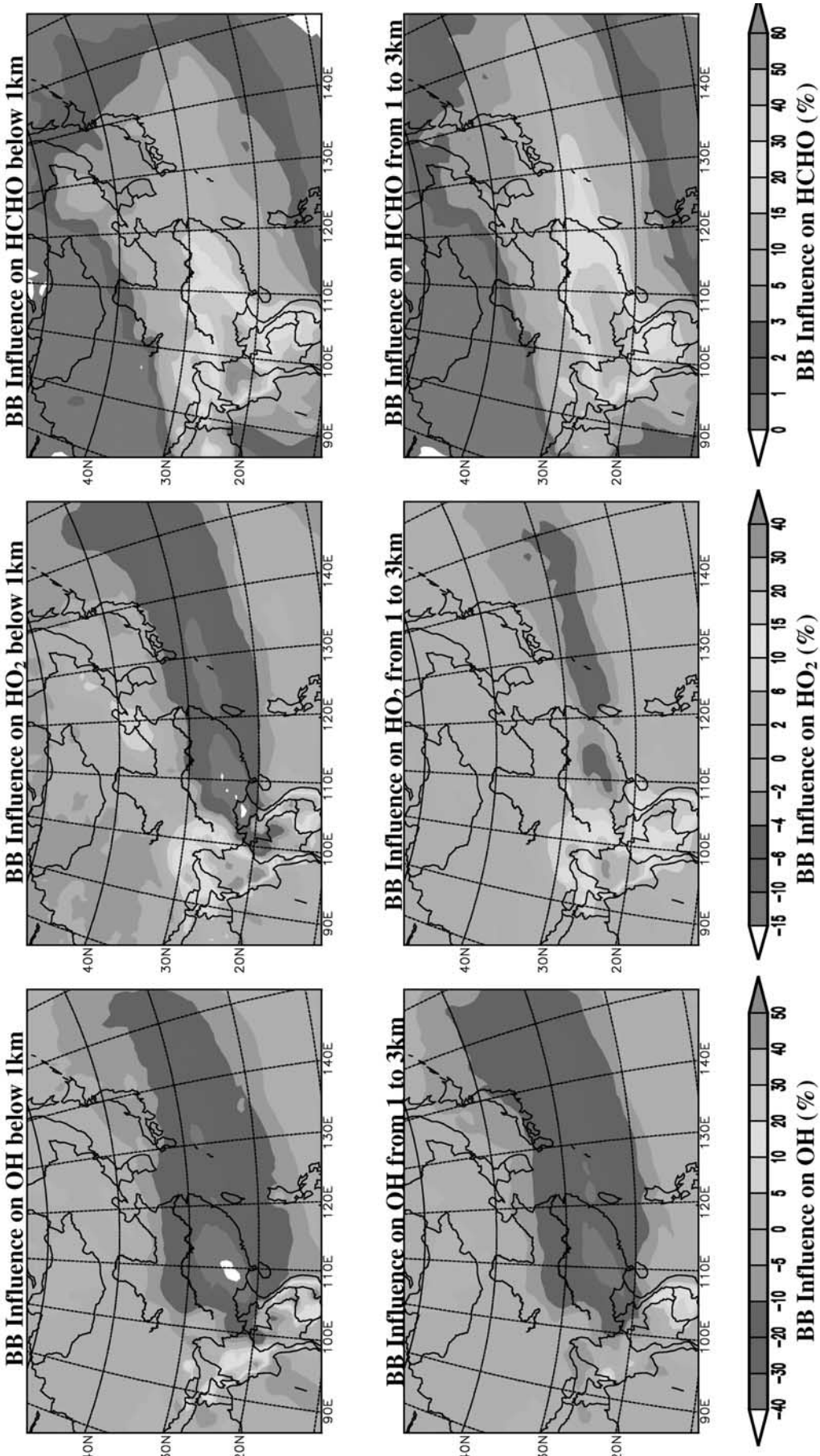

Figure 7. March-averaged biomass burning net influences on daytime OH, HO_2, and formaldehyde for the layers below 1 km and from 1 to 3 km, represented as percentage change. See color version of this figure at back of this issue.

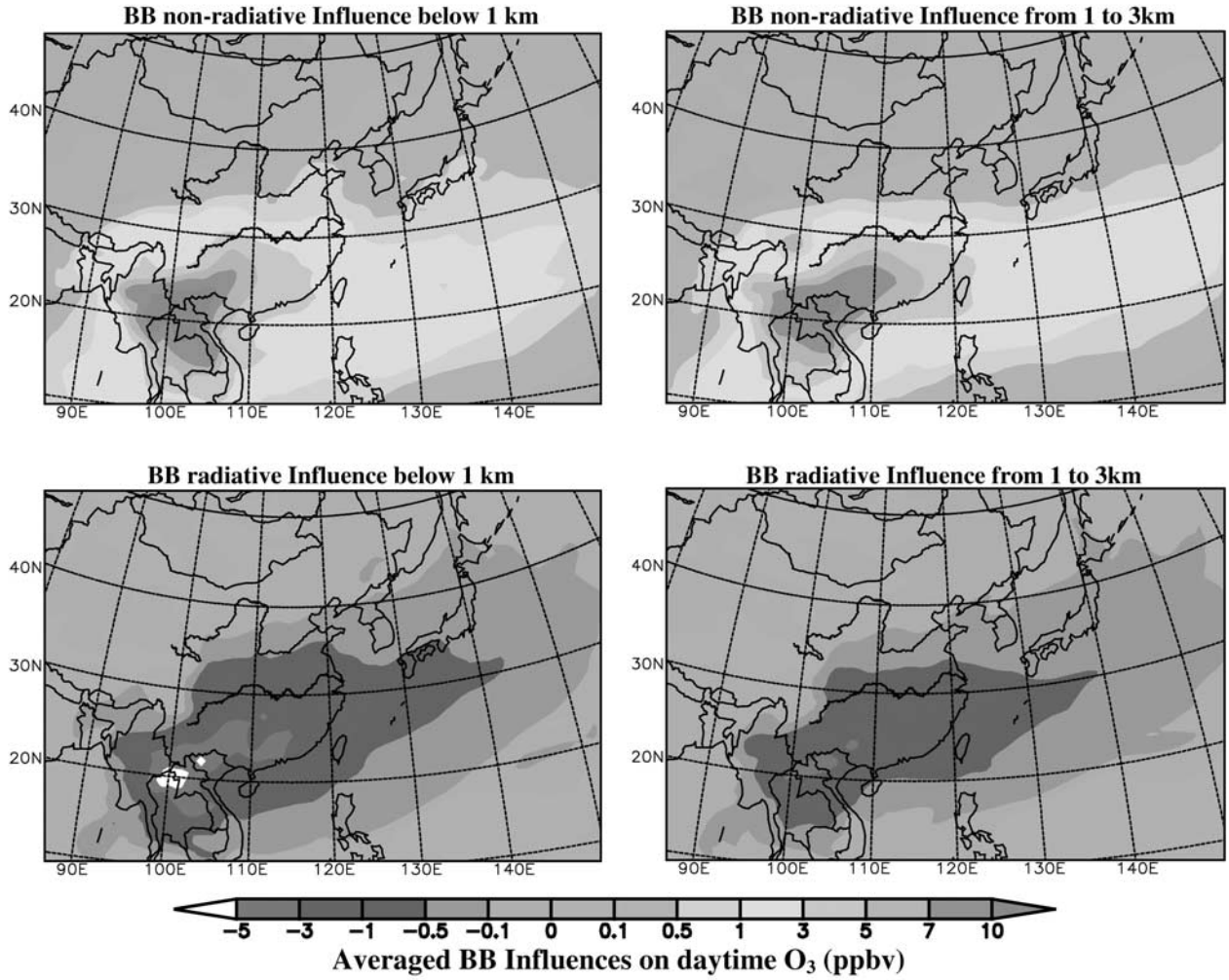

Figure 8. March-averaged biomass burning radiative and nonradiative influences on daytime O_3 for the layers below 1 km and from 1 to 3 km. See color version of this figure at back of this issue.

where the O_3 concentration increases generally by more than 2 ppbv, and occasionally by up to 15 ppbv (Figure 5d). Our study shows that this enhancement can extend up to 8 km altitude along the transport route.

7. Conclusion

[30] This study used the three-dimensional chemical model, STEM 2K1, to retrieve the impacts of biomass burning in east Southeast Asia during the TRACE-P period. By using CO as the main indicator, the modeled results agree with both surface observations and TRACE-P airborne measurements. The sensitivity study enabled us to identify nine periods with significant biomass burning influences from a total of 24 TRACE-P flights. Through studying these nine scenarios, we described the main features of BB CO outflow from Southeast Asia. In this outflow, the biomass burning forms a widespread region where the CO concentrations are enhanced by more than 30 ppbv. In the warm conveyor belt of frontal systems, the exported BB CO concentration can reach up to 500 ppbv. Among the nine BB-affected scenarios, eight were associated with frontal activities.

[31] Using these simulations, we sampled the biomass burning signals quantitatively. Through analyzing the observed data in the biomass burning events, the characteristics of the biomass air masses from Southeast Asia were identified. The Southeast Asia BB air masses contains fewer nitrogen oxidants, but larger amounts of HCN and NMHC (nonmethane hydrocarbon). The BB ratios are higher on $\Delta HCN/\Delta CO$ (0.0015), and $\Delta C_2H_2/\Delta CO$ (0.0036), and lower on $\Delta NO_y/\Delta CO$ (0.005) than those reported from Australian tropical savannas fire [*Hurst et al.*, 1994].

[32] Biomass burning imposes complex influences on regional tropospheric chemistry, which can be divided into radiative and nonradiative influences. The complexity arises even more when the BB plumes interact with biogenic and anthropogenic emissions. Owing to the low OH background constrained by the strong biogenic emissions, the BB gas-phase compounds mainly contribute to OH production consumption in Southeast Asia. Our analysis showed that the BB nonradiative processes also increase the HO_2, HCHO, and O_3 concentrations in the lower troposphere. The BB radiative influences contribute to OH, HO_2, and O_3 reduction, but increased HCHO concentrations by reducing its photolytic loss. Arranged by the sensitivity to the *J* value

change caused by BB aerosols, we found that OH > HO_2 > HCHO > O_3 in regional average. Averaged over March, the biomass burning net influences reach up to 50% for OH, 40% for HO_2, 60% for HCHO, and 10 ppbv for O_3 below 1 km. These highest influences usually appear in biomass burning areas or their adjacent downwind sites.

[33] These results confirm the impact role that biomass burning plays in the chemistry and pollutant outflows in Asia. These results also point out the need to take into account both aerosol and gas-phase chemical processes. These findings underscore the need to further quantify and refine our estimate of biomass burning emissions.

[34] **Acknowledgments.** This work was supported by NASA GTE TRACE-P, ACMAP, and NSF Atmospheric Chemistry program. The Thailand surface data were collected by Air Quality and Noise Management Division, Pollution Control Department, Ministry of Natural Resources and Environment, Thailand.

References

Carmichael, G. R., et al., Regional-scale chemical transport modeling in support of intensive field experiments: Overview and analysis of the TRACE-P observations, *J. Geophys. Res.*, *108*(D21), 8823, doi:10.1029/2002JD003117, in press, 2003.

Galanter, M., H. Levy II, and G. R. Carmichael, Impacts of biomass burning on tropospheric CO, NO_x, and O_3, *J. Geophys. Res.*, *105*(D5), 6633–6653, 2000.

Holloway, T., H. Levy II, and P. Kasibhatla, Global distribution of carbon monoxide, *J. Geophys. Res.*, *105*(D10), 12,123–12,147, 2000.

Hurst, D. F., D. W. T. Griffith, and G. D. Cook, Trace gas emissions from biomass burning in tropical Australian savannas, *J. Geophys. Res.*, *99*(D8), 16,441–16,456, 1994.

Maloney, J. C., H. E. Fuelberg, M. A. Avery, J. H. Crawford, D. R. Blake, B. G. Heikes, G. W. Sachse, S. T. Sandholm, H. Singh, and R. W. Talbot, Chemical characteristics of air from different source regions during the second Pacific Exploratory Mission in the Tropics (PEM-Tropics B), *J. Geophys. Res.*, *106*(D23), 32,609–32,625, 2001.

Reiner, T., D. Sprung, C. Jost, R. Gabriel, O. L. Mayol-Bracero, M. O. Andreae, T. L. Campos, and R. E. Shetter, Chemical characterization of pollution layers over the tropical Indian Ocean: Signatures of emissions from biomass and fossil fuel burning, *J. Geophys. Res.*, *106*(D22), 28,497–28,510, 2001.

Singh, H. B., et al., In situ measurements of HCN and CH_3CN over the Pacific Ocean: Sources, sinks, and budgets, *J. Geophys. Res.*, *108*(D20), 8795, doi:10.1029/2002JD003006, in press, 2003.

Streets, D., et al., An inventory of gaseous and primary aerosol emissions in Asia in the year 2000, *J. Geophys. Res.*, *108*(D21), 8809, doi:10.1029/2002JD003093, in press, 2003.

Tang, Y., et al., Impacts of aerosols and clouds on photolysis frequencies and photochemistry during TRACE-P: 2. Three-dimensional study using a regional chemical transport model, *J. Geophys. Res.*, *108*(D21), 8822, doi:10.1029/2002JD003100, in press, 2003.

Trainer, M., et al., Correlation of ozone with NO_y in photochemically aged air, *J. Geophys. Res.*, *98*(D2), 2917–2925, 1993.

Wang, T., A. J. Ding, D. Blake, W. Zahorowski, C. N. Poon, and Y. S. Li, Chemical characterization of the boundary layer outflow of air pollution to Hong Kong during February–April 2001, *J. Geophys. Res.*, *108*(D20), 8787, doi:10.1029/2002JD003272, in press, 2003.

Woo, J. H., et al., Contribution of biomass and biofuel emissions to trace gas distributions in Asia during the TRACE-P experiment, *J. Geophys. Res.*, *108*(D21), 8812, doi:10.1029/2003JD003200, in press, 2003.

D. R. Blake, Department of Chemistry, University of California at Irvine, Irvine, CA 92697, USA. (drblake@uci.edu)

G. R. Carmichael, Y. Tang, N. Thongboonchoo, and J.-H. Woo, Center for Global and Regional Environmental Research, University of Iowa, 402 Iowa Advanced Technology Laboratories, Iowa City, IA 52242, USA. (gcarmich@icaen.uiowa.edu; ytang@cgrer.uiowa.edu; nthongbo@cgrer.uiowa.edu; woojh21@cgrer.uiowa.edu)

Y. Kondo, Research Center for Advanced Science and Technology, University of Tokyo, 4-6-1 Komaba, Meguro-ku, Tokyo 153-8904, Japan. (kondo@atmos.rcast.u-tokyo.ac.jp)

G. Kurata, Department of Ecological Engineering, Toyohashi University of Technology, Toyohashi, Aichi 441-8580, Japan. (kurata@eco.tut.ac.jp)

H. B. Singh, NASA Ames Research Center, Mail Stop 245-5, Moffett Field, CA 94035, USA. (hanwant.b.singh@nasa.gov)

D. G. Streets, Argonne National Laboratory, DIS/900, 9700 South Cass Avenue, Argonne, IL 60439, USA. (dstreets@anl.gov)

R. W. Talbot, Institute for the Study of Earth, Oceans, and Space, University of New Hampshire, 39 College Road, Morse Hall, Durham, NH 03824, USA. (robert.talbot@unh.edu)

I. Uno, Research Institute for Applied Mechanics, Kyushu University, Kasuga, Fukuoka, 816-8580, Japan. (iuno@riam.kyushu-u.ac.jp)

T. Wang, Department of Civil and Structural Engineering, Hong Kong Polytechnic University, Hung Hom, Kowloon, Hong Kong, China. (cetwang@polyu.edu.cn)

R. J. Weber, School of Earth and Atmospheric Sciences, Georgia Institute of Technology, 221 Boddy Dodd Way, Atlanta, GA 30332, USA. (rweber@eas.gatech.edu)

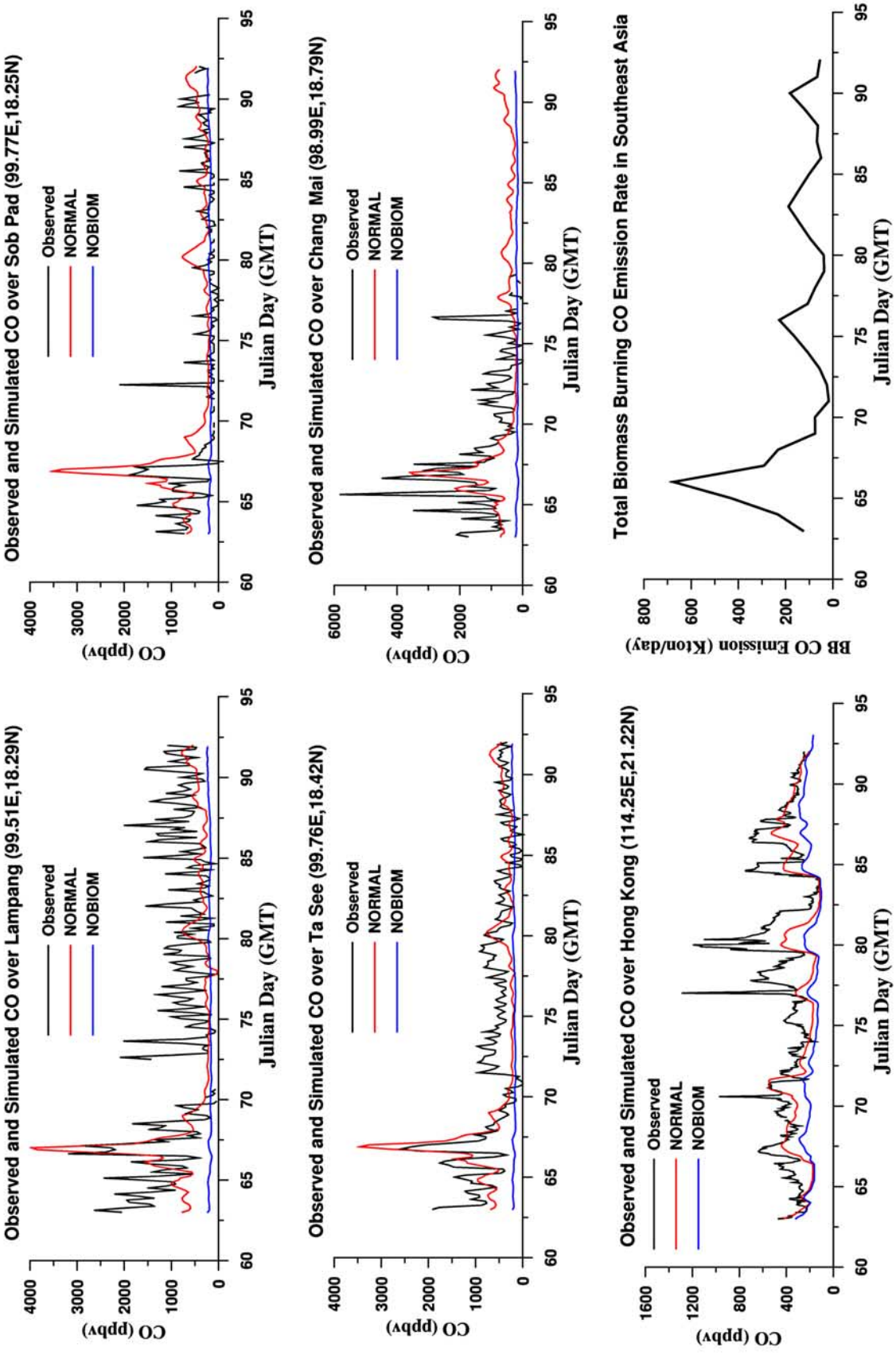

Figure 1. Observed and simulated CO concentrations over four Thailand surface stations and Hong Kong and estimated biomass CO emissions in Southeast Asia during the TRACE-P period. The Lampang, Sob Pad, and Ta See surface stations are located in rural sites, and the Chang Mai and Hong Kong stations are the suburban sites.

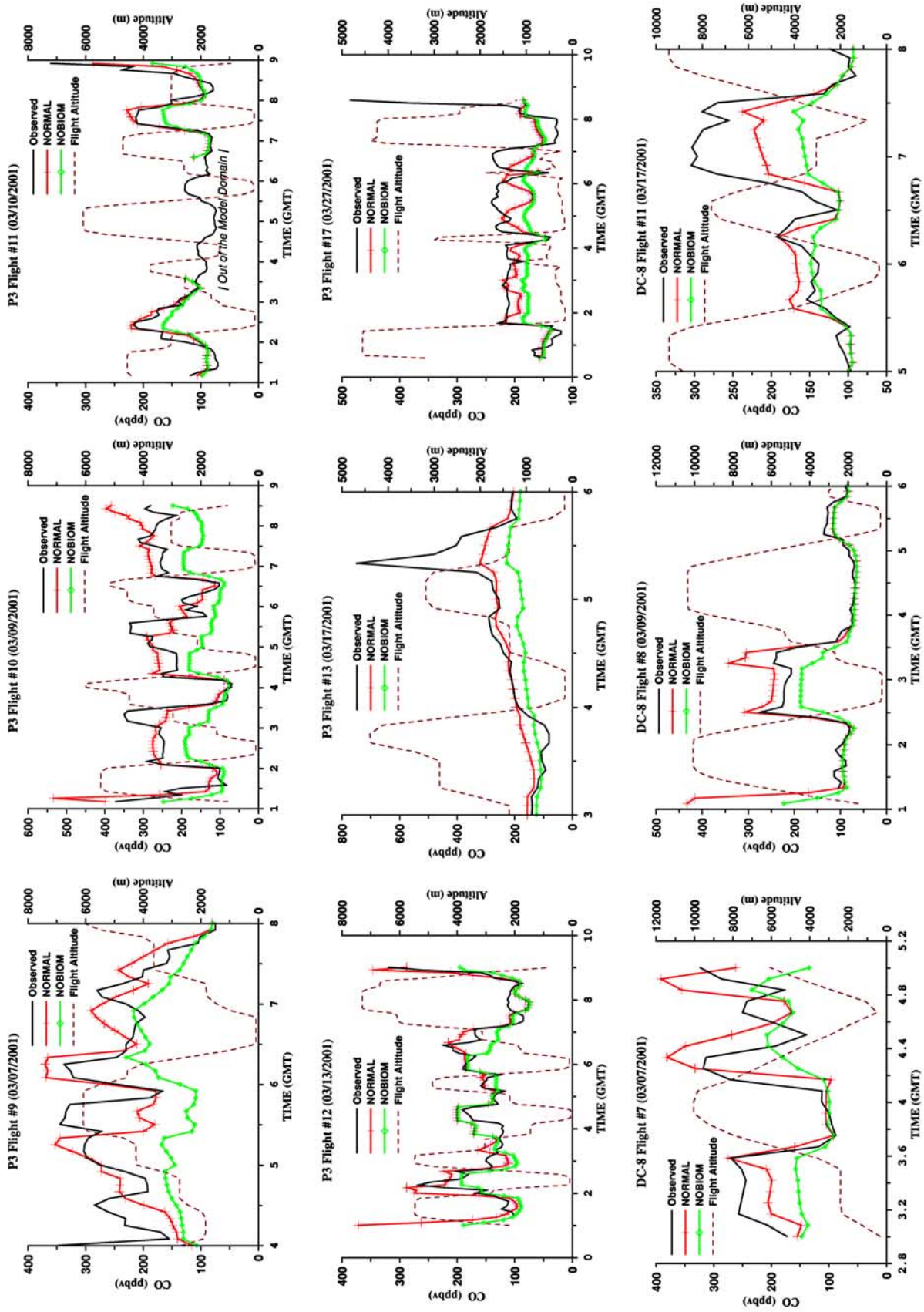

Figure 2. Observed CO compared to NORMAL and NOBIOM simulations for flight segments identified as high-biomass influences.

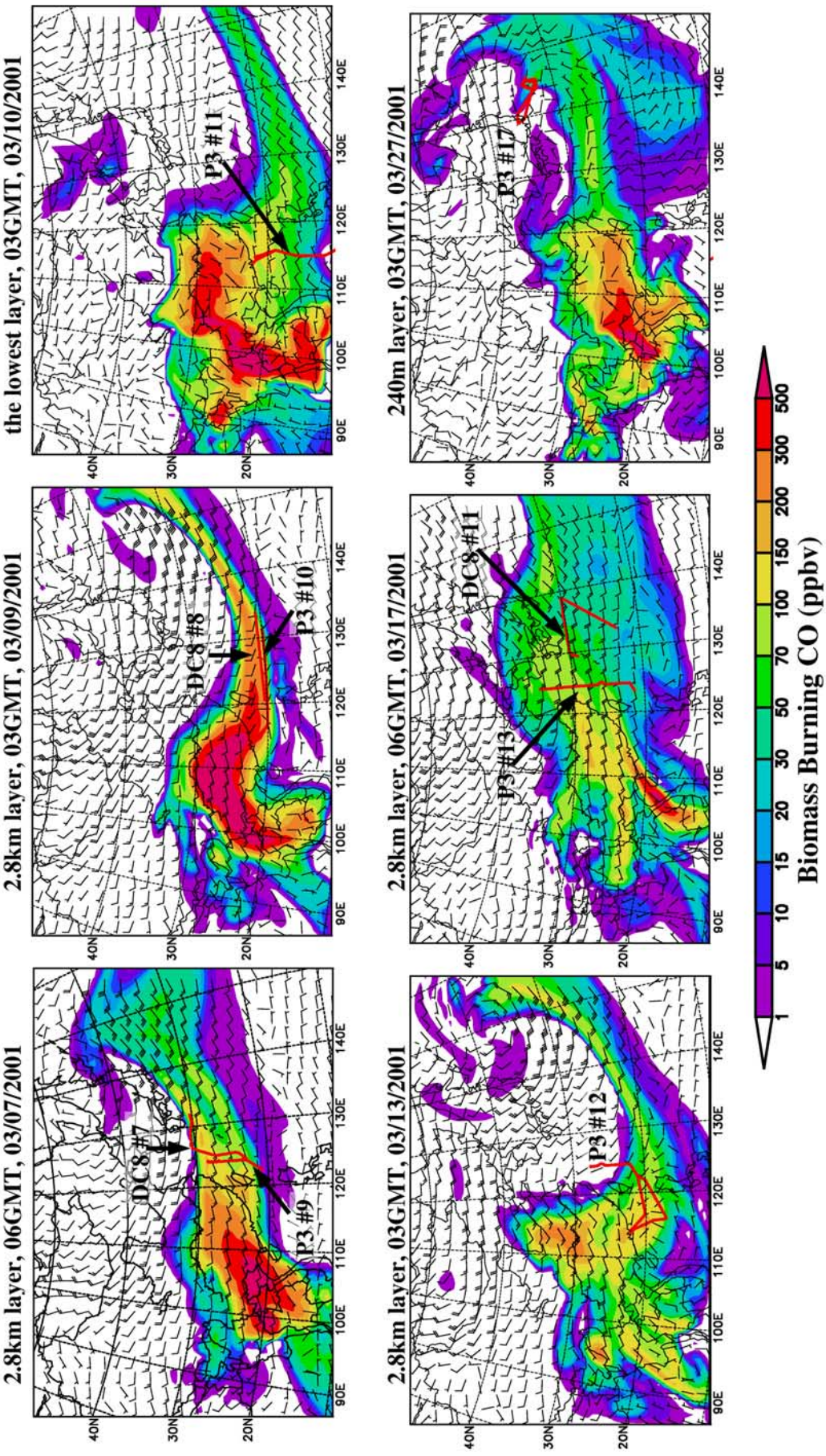

Figure 3. Simulated biomass burning CO concentrations at the major altitudes for the nine flights shown in Figure 2. The red lines refer to the flight paths mentioned in Figure 2.

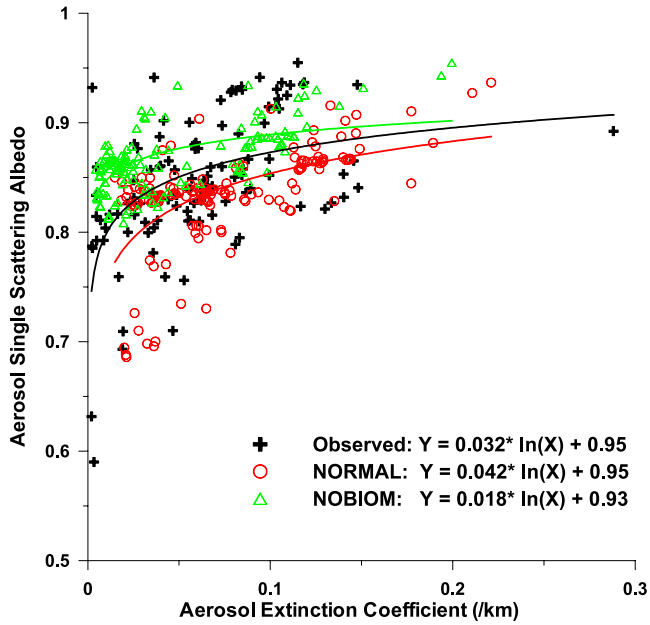

Figure 6. The observed and simulated correlations between aerosol single scattering albedo and extinction coefficient during the biomass burning events (BB CO > 60 ppbv).

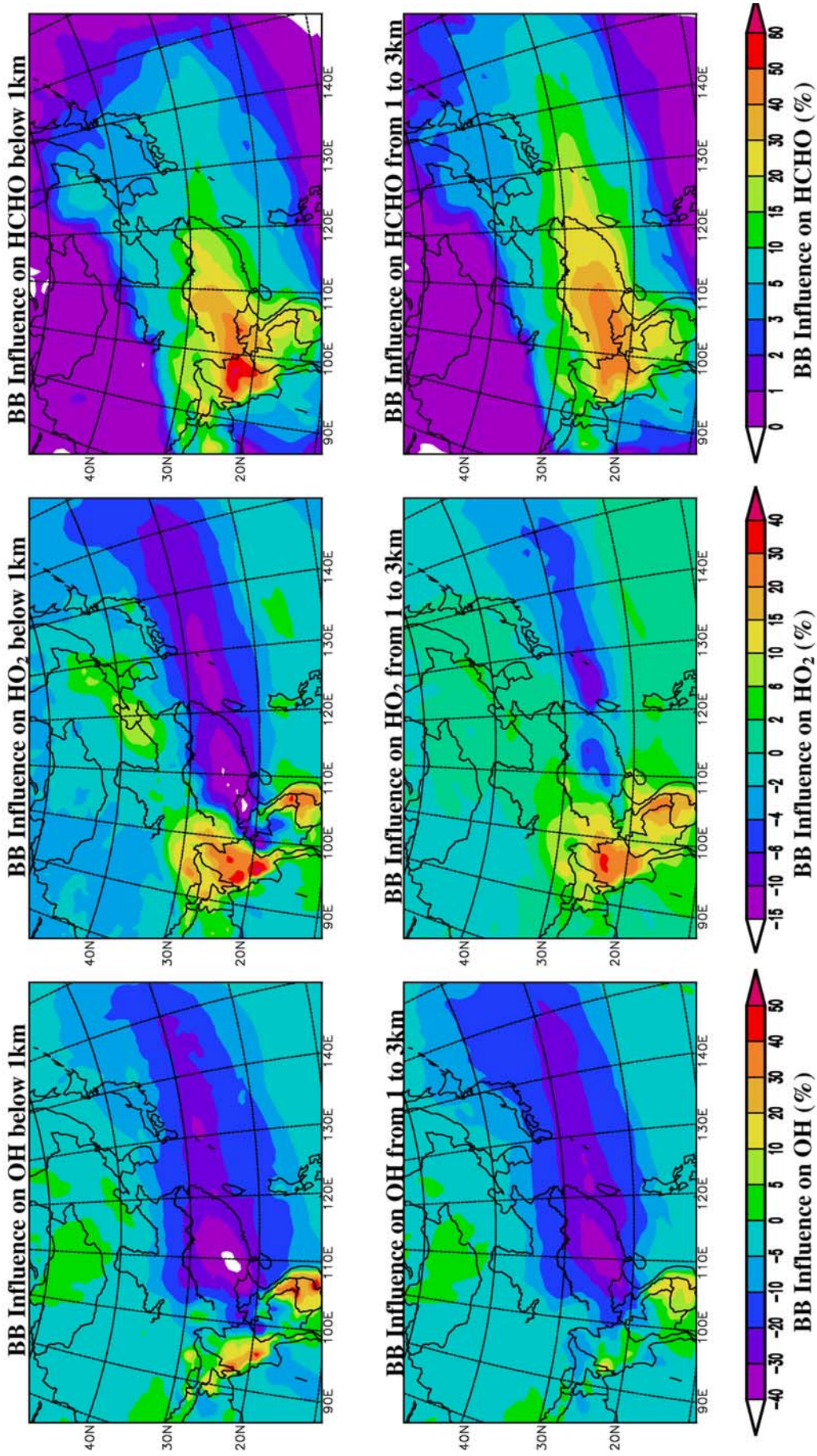

Figure 7. March-averaged biomass burning net influences on daytime OH, HO_2, and formaldehyde for the layers below 1 km and from 1 to 3 km, represented as percentage change.

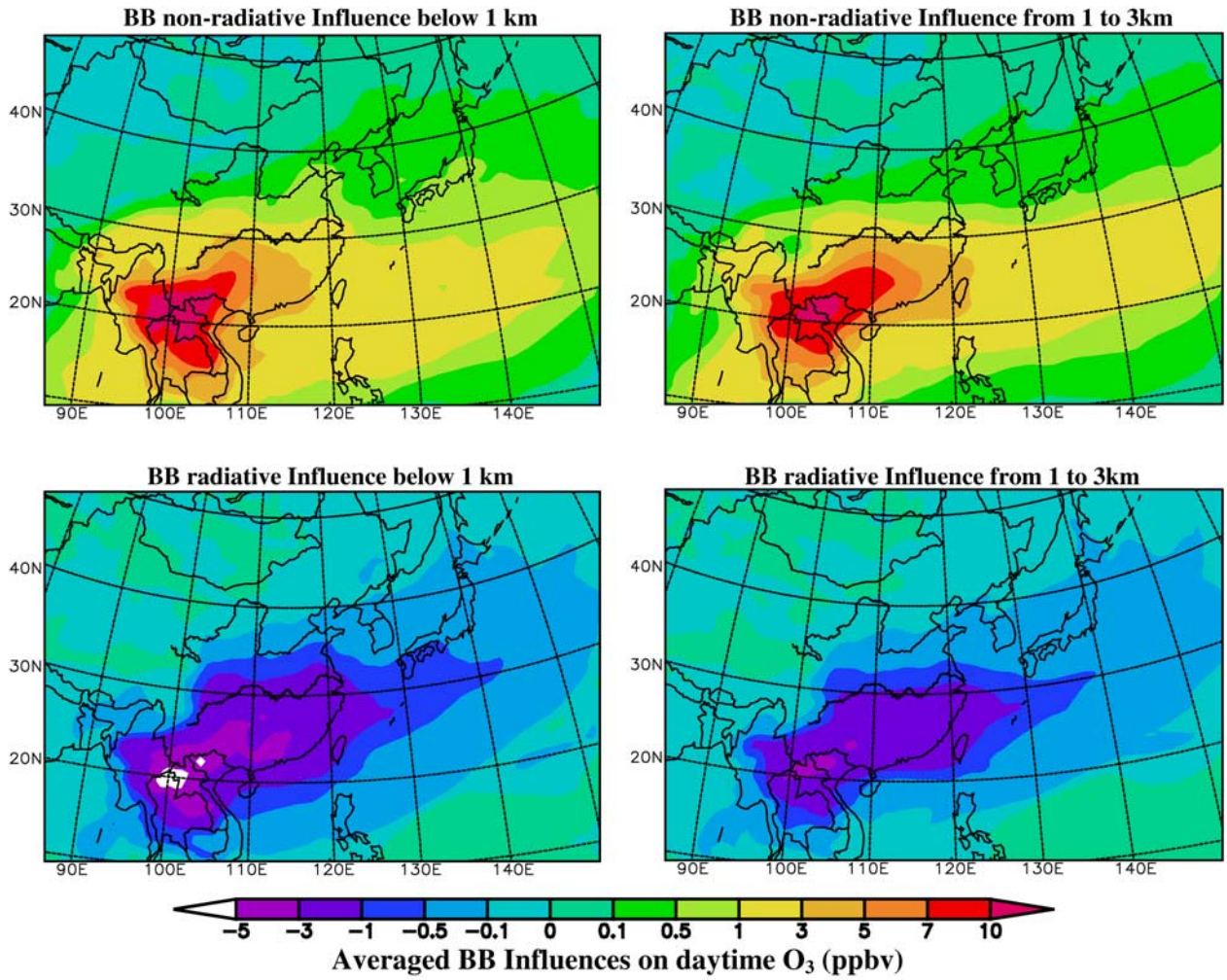

Figure 8. March-averaged biomass burning radiative and nonradiative influences on daytime O_3 for the layers below 1 km and from 1 to 3 km.